Journal of Sciences, Islamic Republic of Iran 33(3): 233 - 243 (2022) http://jsciences.ut.ac.ir
University of Tehran, ISSN 1016-1104

Balangu/Fe_3O_4/Ag_2S/Polyurethane as an Innovative Bio-Nanocomposite Hydrogel: Synthesis, Characterization, Swelling and Drug Delivery Capacity

F. Sheikhshoaii[1], S. Fozooni[2*], H. Hamidian[1]

[1] *Department of Chemistry, Payame Noor University (PNU),19395-4697, Tehran, Islamic Republic of Iran*
[2] *Department of Chemistry, Faculty of science, Shahid Bahonar University of Kerman, 7616913439, Kerman, Islamic Republic of Iran*

Received: 13 August 2022 / Revised: 26 October 2022 / Accepted: 6 November 2022

Abstract

The primary interest of researchers from biology, physics, medicine, chemistry, industry, and material science towards nanotechnology is the most upgrading of production methods, especially those that are cleaner and simpler. This work investigates a new Balangu-based nanocomposite made from Balangu, polyurethane, iron oxide (Fe_3O_4) and silver sulfide (Ag_2S) nanoparticles. The bio-nanocomposite was prepared by the synthesis of Fe_3O_4 and Ag_2S nanoparticles on the Balangu matrix. Balangu is a natural and abundant, renewable polysaccharide, safe to use, non-toxic, hydrophilic, and biodegradable polymer. A mixture of Balangu/Fe_3O_4/Ag_2S nanocomposite hydrogel and ethylene glycol was stirred at ambient temperature. After 2h, diphenyl methane diisocyanate was added and refluxed. The resulted product was filtered and washed thrice with deionized water. Subsequently, Balangu/Fe_3O_4/Ag_2S/polyurethane nanocomposite was obtained by drying in the oven. This research was aimed at investigating the potential of this nanocomposite in drug delivery systems. Balangu/Fe_3O_4/Ag_2S/polyurethane nanocomposite was synthesized using various Ag_2S nanoparticle contents. The resulted bio-nanocomposite was evaluated by FT-IR, XRD, SEM, and TGA techniques. In vitro drug release experiments were performed to assess the efficacy of the developed nanocomposite in the controlled drug delivery systems. The Balangu/Fe_3O_4/Ag_2S/polyurethane nanocomposite containing 0.01 M $AgNO_3$ exhibited longer and better controlled drug release.

Keywords: Balangu; Magnetic nanocomposite; Drug delivery; Swelling; Ag_2S.

Introduction

Biopolymers have recently attracted the attention of researchers as drug delivery systems due to their non-toxicity, biodegradability, and eco-friendly nature. Balangu, also known as Lallemantia royleana, is a

* Corresponding author: Tel: +983431322104; Email: samieh.fozooni@uk.ac.ir; sfozooni2@gmail.com

natural biopolymer that is widely grown in various parts of Europe and the Middle East (Turkey, Iran, and India). This plant is traditionally and industrially used as a beverage [1]. Balangu and its products also have ethnomedicinal applications. Despite few reports on the mechanism of action and phytochemistry of these herbal medicines, growing knowledge has shown the potential of these drugs to treat infectious diseases [2, 3]. A voluminous and transparent mucilage is formed around the black Balangu seeds upon water absorption [4, 5]. As hydrogels are polymeric materials with a high water absorption capacity, this jelly coating was employed to prepare nanocomposite hydrogels. Hydrogels can absorb water in biological environments without being dissolved [6]. High hydrophilicity along with swelling and biocompatibility of hydrogels has introduced them as useful compounds in agriculture [7], pharmaceutical industry [8-10], biosensors [11], tissue engineering [12], and heavy metal sorbents [13, 14]. Organic and inorganic nanocomposite hydrogels have shown unique properties compared to pure polymers. The incorporation of nanoparticles (NPs) can affect the drug release mechanism, reduce the sudden release of the drug, stabilize the drug, and release it continuously and slowly. In this context, iron oxide and silver sulfide nanoparticles were employed to prepare a nanocomposite system. Iron oxide nanoparticles are small [15], low-cost [16], less toxic [17, 18], and easily separable [19] structures which can enter the cell through small capillaries while carrying their drug cargo [20]. Despite their biological applications, metal oxide nanoparticles can lead to drug accumulation in the cell, ending up in inflammation and other adverse effects [21]. Polymer-based nanoparticles can offer the best outcomes by encapsulating drugs and reducing toxicity through limiting their interaction with normal cells. Such systems can present potential benefits such as controlled drug delivery, fewer drug side effects, less frequent drug administration, and the ability to deliver multiple drugs to the same site [22]. Several studies have reported the preparation of nanocomposite hydrogels based on chitosan [23], alginate [24], carrageenan [25], carboxy methylcellulose [26], tragacanth [27], salep [28], starch [29], guar gum [30], psyllium [31], and gum Arabic [32]. Polyurethane was also used in the structure of the novel Balangu/iron oxide/silver sulfide nanocomposite to increase its efficiency. Polyurethane is a versatile polymer with a variety of applications in coatings, adhesives, plastics, elastomers, foams, and composites [33]. Polyurethane has an NCOO bond in its structure that is similar to peptide bonds in proteins. Thanks to this similarity, polyurethane is used in the structure of heart valves, dialysis membranes, and breast implants [34]. In addition, the biomedical application of polyurethane hydrogels has been extensively studied for controlled drug delivery, tissue engineering, wound dressing [35, 36], and heavy metal removal [37, 38]. Regarding the poor hydrophilicity of polyurethane, polyurethane-producing monomers were prepared in the Balangu polyhydroxyl hydrogel substrate, which can be activated with iron oxide and silver sulfide nanoparticles to enhance the hydrophilicity. The structure of the nanocomposite was characterized using IR, SEM, TGA, and XRD techniques. Moreover, its application in drug delivery systems was investigated.

Materials and Methods

1. Materials

Balangu was purchased from the medicinal plants store in Kerman, Iran. acetone, thiourea, silver nitrate, sodium acetate, ferrous chloride ($FeCl_2.4H_2O$), sodium hydroxide, diphenylmethane diisocyanate, ethylene glycol, ferric chloride ($FeCl_3.6H_2O$), thiourea, ethanol, phosphoric acid (98% purity), hydrochloric acid (HCl, 36% purity) and ammonia (NH_3) solution were purchased from Merck, Germany. Propranolol was obtained from Darupakhsh pharmaceutical company.

2. Instrumental Analysis

X-ray powder diffraction (XRD) patterns of the samples were obtained using a Rigaku diffractometer, model X Pert PHILIPS operating on Cu-*K*α radiation. FT-IR spectra of the samples (as KBr pellets) were determined using a Bruker tensor 27 spectrophotometer. SEM images were recorded using VEGA// TESCAN. UV-Vis spectra were recorded utilizing a PG instruments SINTRAGBC6 Spectrophotometer. The thermal degradations were observed by a NETZSCH STA 409 PC/PG thermo-gravimetric analyzer (TG). All analyses were carried out on the sample (with the weight of 5-20 mg) within a temperature range of 25-600 °C at a scan rate of 10 °C/min.

3. Preparation of Balangu gel

The Balangu seeds were first manually cleaned to eliminate any stones, chaffs and dust, stored. Balangu seeds (50 g) were immersed in 500 ml distilled water at room temperature (RT) overnight to extract their mucilage. After the extraction process, the solution was dewatered by acetone and filtered. The mucilage was dried at 50°C for overnight.

4. Synthesis of the Balangu /Fe_3O_4 nanocomposite

The ferrous chloride solution (0.5 M) was prepared

by dissolving 2.48 g $FeCl_2 \cdot 4H_2O$ into HCl (25 ml, 2 M). A solution of $FeCl_3 \cdot 6H_2O$ (0.25 M) was also prepared using 1.69 g $FeCl_3 \cdot 6H_2O$ and HCl (25 ml, 2M). Afterward, 1 ml $FeCl_2 \cdot 4H_2O$ and 4 ml $FeCl_3 \cdot 6H_2O$ solution were added to 30 ml deionized water, followed by 5 minutes of stirring. The obtained solution was titred using 16ml ammonia solution (1 M). The colour of the solution immediately altered from yellowish-brown to dark-brown, showing the formation of magnetite (Fe_3O_4) nanoparticles [39]. Then, 10 g Balangu was added to the mentioned solution and stirred at 70 ˚C for 6 h, resulting in a gelatinous substance which was coagulated with 100ml acetone. Finally, the product was collected with a magnet and dried at 50 ˚C.

5. Synthesis of the Balangu /Fe_3O_4/Ag_2S nanocomposite hydrogel

Thiourea (0.05 g), 12.5 ml aqueous $AgNO_3$ solution (0.01, 0.02, 0.03, 0.04, 0.05M) and 4 ml NaOH was added to 1g Balangu /Fe_3O_4 nanocomposite hydrogel in 50ml deionized water with stirring at 150 rpm and 70˚C for 3h. The obtained Balangu /Fe_3O_4 /Ag_2S nanocomposite was dewatered in acetone. The final product was magnetically collected and dried at 50 ˚C.

6. Synthesis of the Balangu /Fe_3O_4/Ag_2S/polyurethane nanocomposite hydrogel

1g Balangu /Fe_3O_4/Ag_2S nanocomposite hydrogel and 8ml ethylene glycol were added and stirred at RT. After 2h, 2 ml diphenyl methane diisocyanate was added and refluxed at 80 ˚C for 2h. Then 40 ml deionized water was poured into the mixture under vigorous stirring for 30–50 s. The resulted product was filtered and washed thirst with deionized water. Subsequently, Balangu/Fe_3O_4/Ag_2S/polyurethane nanocomposite was obtained by drying in the oven at 50˚C.

7. Swelling Measurement

0.5 gr nanocomposites were transferred to a teabag and immersed in 100 ml double-distilled water at 37 ºC. After hanging up the teabag for 5 min for the removal of the excess solution, its weight was measured until reaching a stable weight. The swelling was determined by the following equation:

$$\text{Swelling ratio} = \frac{w2-w1}{w1}$$

W_1 = Initial sample weight

W_2 = The weight of the sowallen sample

8. Drug loading and drug release behaviour

The nanocomposite sample (1 g) was immersed in 100 mL of propranolol solution 2.5% for 24 h. The sample was then taken out from the solution and kept for drying. The release studies of drugs were carried out spectrophotometrically at a characteristic λmax (214 nm) using a calibration curve obtained from a series of propranolol solutions with known concentrations. The concentration of the released drug was investigated at pH = 7.4, T= 37 ˚C and different time intervals.

Results and Discussion

Structural models of Balangu/ Fe_3O_4/ Ag_2S/ polyurethane nanocomposite are proposed in Schemes 1 and 2. As seen, Fe_3O_4 and Ag_2S modified Balangu with are covalently connected with polyurethane to become a constituent part of the polyurethane molecules. The structure of the nanocomposite was characterized by spectral analysis [40-42].

1. FTIR spectroscopy Balangu/Fe_3O_4 and Balangu/Fe_3O_4/Ag_2S / polyurethane

The IR spectrum of nanocomposite Balangu/Fe_3O_4 showed the bonds belonging to Balangu hydroxyl group and C=C at 3422.42 and 1616.86 cm^{-1} respectively. The peak at 614.14 cm^{-1} has corresponded to the Fe-O stretching vibrations. The IR spectrum of nanocomposites confirmed the presence of the Balangu and polyurethane hydroxyl groups and amidic NH at 3373.66 cm^{-1}abroudly. The polyurethane carbonyl group and C=C emerged at 1702.8 and 1617.07 cm^{-1}, while the peaks at 615.82 and 506.63 cm^{-1} have corresponded to the Fe-O stretching vibrations (Figure 1).

2. X-ray diffraction

Figure 2 shows the XRD results of the Balangu/Fe_3O_4/Ag_2S/polyurethane hydrogel for 2θ=2–70°. The peaks related to the Fe_3O_4 crystals emerge at 2θ ~ 30°, 36°, 43°, 54°, 57°, 63° while those associated with Ag_2S nanoparticles appear at 2θ=29°, 31°, 34°, 37°, 41°, 43°. All the peaks well coincided with those of Fe_3O_4 and Ag_2S crystals, confirming the synthesis of Fe_3O_4 and Ag_2S nanoparticles in the Balangu matrix. A broad peak at 22.5° is due to the polymer networks [43].

3. Scanning electron microscopy (SEM)

SEM images of the Balangu/Fe_3O_4, Balangu/ Fe_3O_4/ Ag_2S, and Balangu/ Fe_3O_4/ Ag_2S/ polyurethane nanocomposites are depicted in Figure 3a-d. The morphological changes of Balangu/Fe_3O_4 are studied after the incorporation of Ag_2S NPs as well as the co-polymerization of ethylene glycol and diphenylmethane

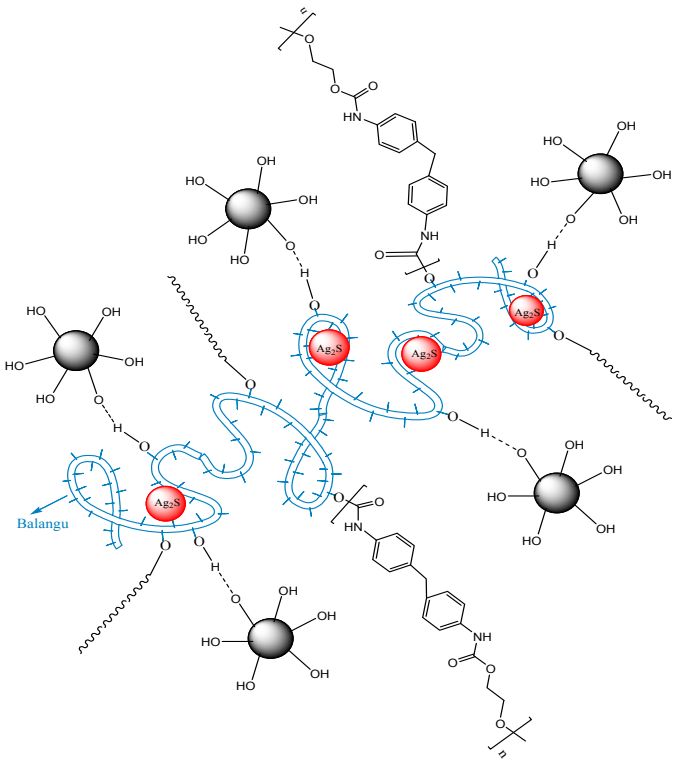

Scheme 1. schematic representation of Balangu/Fe_3O_4/Ag_2S/Polyurethane nanocomposite hydrogel

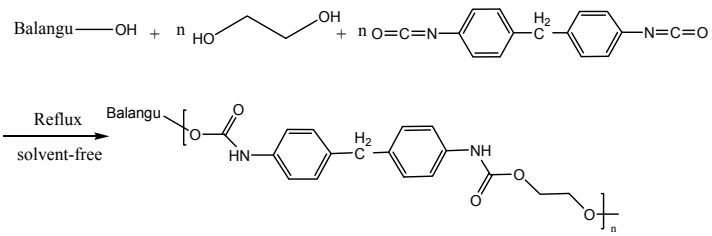

Scheme 2. The plausible formation process of Balangu/Fe_3O_4/Ag_2S/Polyurethane nanocomposite hydrogel.

diisocyanate within the Balangu/Fe_3O_4/Ag_2S matrix. Thanks to its wide surface area, Balangu acts as a bed/support for Fe_3O_4 and Ag_2S NPs. Based on Figure 3a, Fe_3O_4 nanoparticles showed proper dispersion in the Balangu matrix with particles size less than 50 nm. After the incorporation of Ag_2SNPs, more particles that are spherical were formed in the structure of the nanocomposites. Figure 3c shows a slight change in the surface morphology of the nanocomposite after coating with polyurethane. Figure 3d (75.00 kX) also indicates the presence of nanoparticles smaller than 100 nm. Finally, the SEM image proves the presence of voids and the highly porous structure of nanocomposites, introducing a promising carrier for drug delivery systems.

4. Thermogravimetric analysis (TGA)

The TGA diagrams of Balangu-based nanocomposites are illustrated in Figure 4. By introducing Fe_3O_4 to Balangu, the initial decomposition temperatures increased from 280°C to 320 °C. The synthesis of Ag_2S in the Balangu/Fe_3O_4 matrix led to no further improvement in initial decomposition temperature. The TGA curve of Balangu/ Fe_3O_4/ Ag_2S/ polyurethane showed a higher mass loss at 200–600 °C compared to the three other nanocomposites, indicating the successful grafting of the polymer onto the Balangu/ Fe_3O_4/ Ag_2S structure. The improvement in thermal stability of Balangu/ Fe_3O_4/ Ag_2S/ polyurethane can be attributed to the compatibility between the Balangu hydrogel network and the polyurethane chains [44, 45].

5. Swelling studies

Hydrogels have found increasing popularity in numerous fields. In this research, swelling increased with an increase in $AgNO_3$ concentration from 0 to 0.01

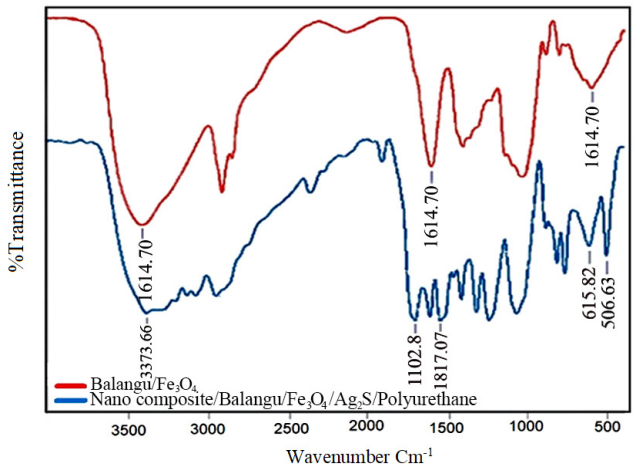

Figure 1. FTIR spectra of Balangu/Fe_3O_4 and Balangu/Fe_3O_4/Ag_2S/polyurethane

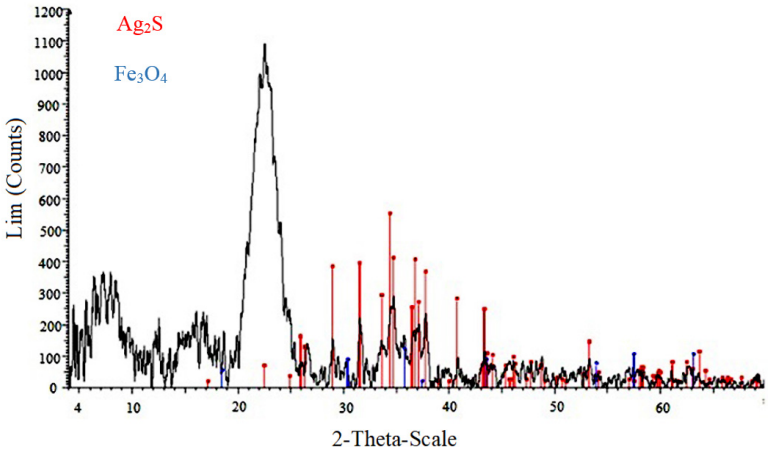

▪ 24-0715 (D) - Acanthine -Ag_2S- Y: 50.00%-dx by: 1.- WL:1.5406 – monoclinic - a 4.23100 - b 6.93000 - c 9.52600 - alpha 90.000 - beta 125.480 – gamma 90.000 – primitive - P21/c (14) – 4 - 227.447. l/lc pdf 1. Sq 82.8%
▪ 11-0614 (D) - Magnetite - Fe_3O_4- Y: 10.42%-d x by: 0.9917-WL: 1.54.6 – cubic -a 8.39630 - b8.39630 – c8.39630- alpha 90.000- beta 90.000 - gamma 90.000 – Face – centred- Fd^3m (227) - 8-591.921- l/lc pdf 1. l/lc use

Figure 2. The XRD patterns of Balangu/ Fe_3O_4/ Ag_2S/ polyurethane

M and then decreased (Table S1, Figure 5). The increment in the swelling capacity of the nanocomposite hydrogels can be assigned to the presence of Ag_2S nanoparticles. The formation of Ag_2S in the hydrogel can expand the hydrogel network and enhance its free space and pores. Therefore, Balangu/ Fe_3O_4/Ag_2S/polyurethane samples adsorb more water (Fig. S1). However, increasing of $AgNO_3$ revealed less swelling capacity. This can be assigned to the knot-tying role of Ag_2S NPs, that inhibits the extension of polymer chains. The knot-tying effect of Ag_2S can be attributed to the chelation of Fe_3O_4 and some hydroxyl groups of the hydrogel networks with Ag_2S NPs.

6. Drug loading and release behaviours of nanocomposite

The propranolol release profile (Fig S2) was investigated to show the drug delivery potential of Balangu/ Fe_3O_4/ Ag_2S/polyurethane nanocomposites. The relationship between propranolol encapsulation and release was assessed by changing the level of Ag_2S NPs. The calibration curve of propranolol is shown in Fig S3. Table S2 and Figure 6 present the release rate of propranolol at 214.83 nm as a function of time (Fig S4).

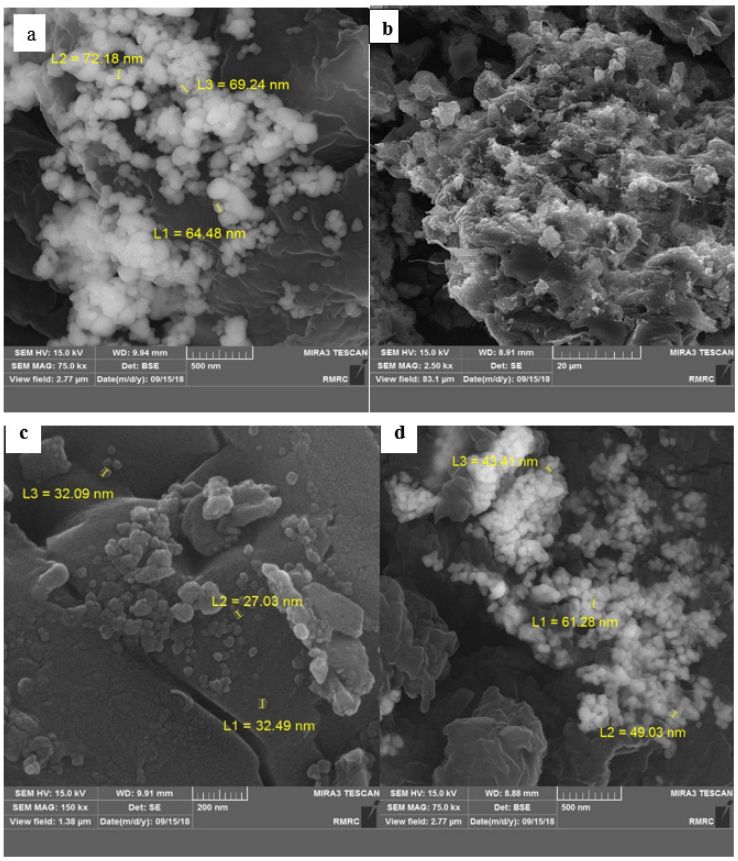

Figure 3. SEM images of (a) Balangu/Fe_3O_4, (b) Balangu/Fe_3O_4/Ag_2S nanocomposites, (c) Balangu/ Fe_3O_4/Ag_2S/polyurethane nanocomposite (SEM MAG: 2.50kx), (d) Balangu/Fe_3O_4/Ag_2S/polyurethane nanocomposite (SEM MAG: 75.0kx)

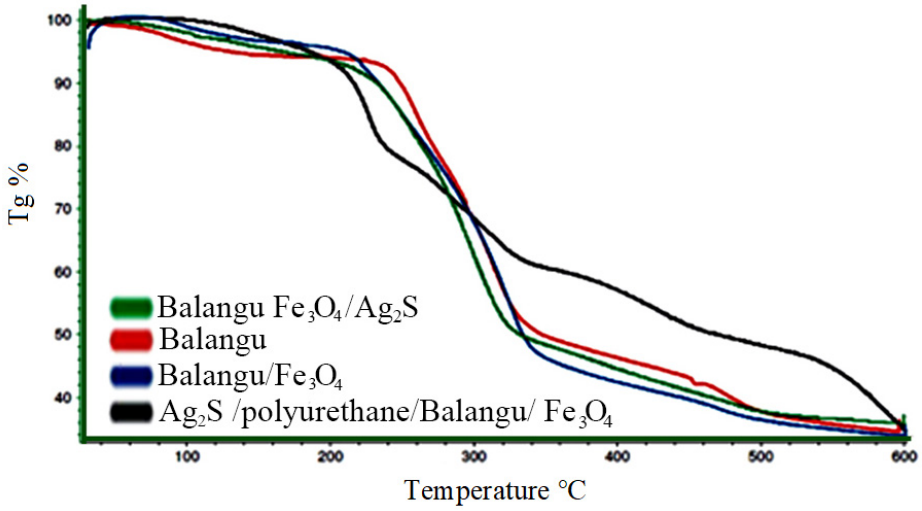

Figure 4. TGA thermograms of Balangu based nanocomposites

As observed, the more the content of Ag_2S nanoparticles, the less the drug release. This trend can be due to the presence of nanoparticles with a significant impact on slow drug release from the nanocomposite hydrogels. Drug release profile of the nanocomposite hydrogels at pH = 7.4 reveals that higher drug release from Ag_2S-free hydrogel compared to other nanocomposite hydrogels.

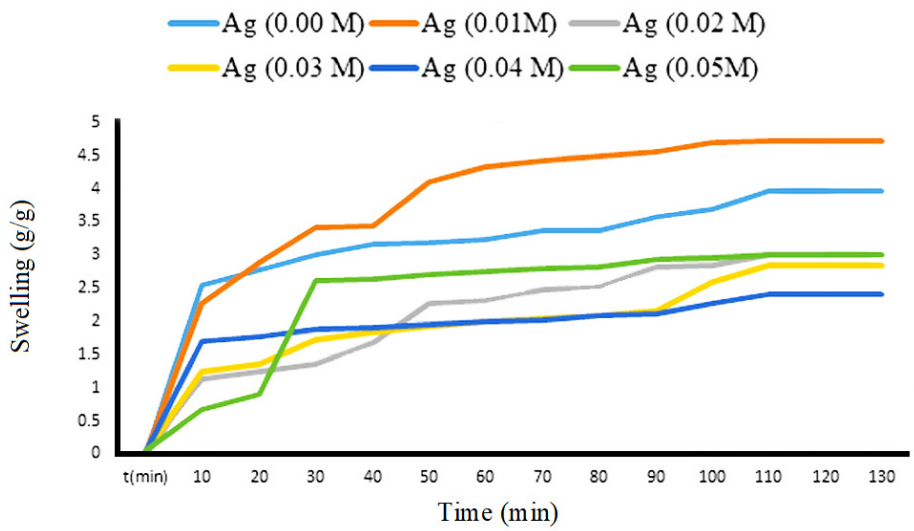

Figure 5. Swelling profile of Balangu/ Fe_3O_4/Ag_2S/polyurethane in different time

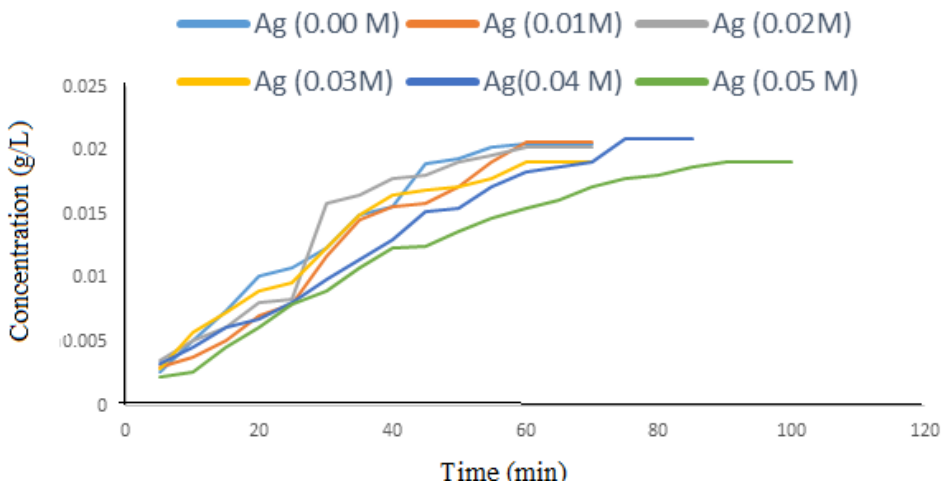

Figure 6. Drug release behaviour of Balangu/ Fe_3O_4/ Ag_2S/ polyurethane nanocomposite at pH 7.4 and 37 °C.

Conclusion

In this work, Balangu/ Fe_3O_4/Ag_2S/polyurethane nanocomposite hydrogel was synthesized using a combination of Fe_3O_4 and Ag_2S NPs and Balangu biopolymer for swelling, drug delivery, and heavy metal removal purposes. Structural characterizations were achieved by IR, XRD, TG, and SEM techniques. SEM results showed the formation of nanoparticles in the size range of 20 to 80 nm. XRD analysis also confirmed the growth of Fe_3O_4 and Ag_2S NPs in the hydrogel matrix. In vitro, propranolol drug release was investigated using a nanocomposite. Higher and faster drug release was observed in initial times which decreased over time. The effect of Ag_2S NPs on the swelling and drug release of the nanocomposite was also explored. The prolonged release time of drug molecules can be assigned to a longer migration path of the drugs from the nanocomposite to the medium. According to the results, the proposed Balangu/Fe_3O_4/Ag_2S/Polyurethane nanocomposite hydrogel can serve as a promising platform in controlled drug delivery purposes.

Declaration of conflicting interests

The authors confirm that there are no potential conflicts of interest in the research, authorship, and /or

publication of this paper.

Acknowledgements

The authors appreciate the cooperation of the Payame Noor University of Kerman and Department of Chemistry, Shahid Bahonar University of Kerman for supporting this investigation.

References

1. Razavi SMA, Mohammadi MT. Influence of different substitution levels of Balangu Seed gum on textural characteristics of selected hydrocolloids. Elec. J. Environ. Agric. Food. Chem. 2011;10: 2676-2688.
2. Dogruoz N, Zeybek Z, Karagoz A. Antibacterial activity of some plant extracts. IUFS J. Biol. 2008; 67: 17–21.
3. Samee H, Li Z, Lin ZH, Khalid J, Guo Y. Anti-allergic effects of ethanol extracts from brown seaweeds. Univ. Sci B. 2009;10:147-153.
4. Naebi M, Torbati M A, Azadmard-Damirchi S, Siabi S, Savage GP. Changes in physicochemical properties of cold press extracted oil from Balangu (Lallemantia peltata) seeds during storage. J. Food Compos. Anal. 2022; 107: 104358.
5. Amini AM, Razavi S. Dilute solution properties of Balangu (Lallemantia royleana) seed gum: effect of temperature, salt, and sugar. Int. J. Biol. Macromo. 2012;51: 235–243.
6. Namazi H, Rakhshaei R, Hamishehkar H, Samadi Kafil H. Antibiotic loaded carboxymethyl cellulose/MCM-41nanocomposite hydrogel films as potential wound dressing. Int. J. Biol. Macromol. 2016;85: 326-334.
7. Singh N, Agarwal S, Jain A, Khan S. 3-Dimensional cross linked hydrophilic polymeric network "hydrogels": An agriculture boom. Agric. Water. Manag. 2021; 253:106939.
8. Bankhede HK, Ganguly A. Pharmaceutical polymer-based hydrogel formulations as prospective bioinks for 3D bio printing applications: A step towards clean bio printing. Annals. 3D. Print. Med. 2022; 6: 100056.
9. Bai S, Niu X, Wang H, Wei L, Liu L, Liu X, Eelkema R, Guo X, Esch J, Wang Y Chemical reaction powered transient polymer hydrogels for controlled formation and free release of pharmaceutical crystals. Chem. Eng. J. 2021;414: 128877.
10. Wei W, Zhao A, Ge K, Zhang C, LiY, Zhang J, Jia G. Monodisperse and mesoporous walnut kernel-like SiO_2/γ-Fe_2O_3 nanocomposite Synthesis, magnetic properties, and application in drug delivery. J Alloys. Comd. 2017; 72825: 585-591.
11. Richter A, Paschew G, Klatt S, Lienig J, Arndt KF, Adler HJP. Review on hydrogel- based pH sensors and microsensors. Sensors. 2008;8: 561–581.
12. Van Vlierberghe S, Dubruel P, Schacht E. Biopolymer-based hydrogels as scaffolds for tissue engineering applications. Biomacromol 2011;12: 1387–1408.
13. Mahmoud ME, Osman MM, Abdel-Aal H, Nabil GM. Microwave-assisted adsorption of Cr(VI), Cd(II) and Pb(II) in presence of magnetic graphene oxide-covalently functionalized-tryptophan nanocomposite.J. Alloys. Comd. 2020; 82315: 153855.
14. Paulino AT, Belfiore LA, Kubota LT, Muniz EC and Tambourgi EB. Efficiency of hydrogels based on natural polysaccharides in the removal of Cd^{2+} ions from aqueous solutions. Chem. Eng. J. 2011;168: 68–76.
15. Li W, Zeng G, Yan J, Liu X, Jiang X, Yang J, Liu J, Sun D. One-pot green synthesis of I@CNDs-Fe_3O_4 hybrid nanoparticles from kelp for multi-modal imaging in vivo. Mater. Sci. Eng. C. 2021;124: 112037.
16. Li T, Yang T, Yu Z, Xu G, Han Q, Luo G, Du J, Guan Y, Guo C. Trivalent chromium removal from tannery wastewater with low cost bare magnetic Fe_3O_4 nanoparticles. Chem. Eng. Process.: Process Intensif. 2021;169: 108611.
17. Braim F S, Razak NNAN, Aziz AA, Ismael L Q, Sodipo B K. Ultrasound assisted chitosan coated iron oxide nanoparticles: Influence of ultrasonic irradiation on the crystallinity, stability, toxicity and magnetization of the functionalized nanoparticles. Ultrason. Sonochem. 2022;88: 106072.
18. Mahmoudi M, Sant S, Wang B, Laurent S, Sen T. Superparamagnetic iron oxide nanoparticles (SPIONs): development, surface modification and applications in chemotherapy. Adv. Drug. Delivery. Rev. 2011;63: 24–46.
19. Ma M, Hou P, Zhang P, Cao J, Liu H, Yue H, Tian G, Feng S. Magnetic Fe_3O_4 nanoparticles as easily separable catalysts for efficient catalytic transfer hydrogenation of biomass-derived furfural to furfuryl alcohol. Appl. Catal. A: Gen. 2020;602: 117709.
20. Vidyanathan R, Kalishwaralal K, Gopalram S, Gurunathan S. Nanosilver the burgeoning therapeutic molecule and its green synthesis. Biotechnol. Adv 2009;27: 924-937.
21. Francis AP, Dushendra Babu GJ, Lavanya M, Shenbaga Vidhy K, Devasena T. Toxicity studies of Aluminium oxide nanoparticles in cell lines. Int. J. Nanotechnol. Appl. 2011;5: 99-107.
22. Muhammed Rafeeq PE, Junise V, Saraswathi R, Krishnan PN, Dilip C. Development and characterization of chitosan nanoparticles loaded with isoniazid for the treatment of Tuberculosis. Res. J. Pharm. Biol. Chem. Sci. 2010;1: 383-390.
23. Bozoğlan BK, Duman O, Tunç S. Preparation and characterization of thermosensitive chitosan/carboxy methylcellulose/scleroglucan nanocomposite hydrogels. Int J Biol Macromol 2020;162: 781-797.
24. You Y, Qu K, Shi C, Sun Z, Huang Z, Li J, Dong M, Guo, Z. Binder-free CuS/ZnS/sodium alginate/rGO nanocomposite hydrogel electrodes for enhanced performance supercapacitors. Int. J. Biol. Macromol. 2020;162: 310-319.
25. Yegappan R, Selvaprithiviraj V, Amirthalingam S, Mohandas A, Hwang NS, kumar RJ. Injectable angiogenic and osteogenic carrageenan nanocomposite hydrogel for bone tissue engineering. Int. J. Biol. Macromol. 2019; 122: 320-328.
26. Rakhshaei R, Namazi H, Hamishehkar H, Rahimi M. Graphene quantum dot cross-linked carboxymethyl cellulose nanocomposite hydrogel for pH-sensitive oral anticancer drug delivery with potential bioimaging properties. Int J Biol Macromol 2020;150: 1121-1129.

27. Mallakpour S, Abdolmaleki A, Tabesh, F. Ultrasonic-assisted manufacturing of new hydrogel nanocomposite biosorbent containing calcium carbonate nanoparticles and tragacanth gum for removal of heavy metal, Ultrason Sonochem 2018;41: 572-581.
28. Bardajee, GR, Hooshyar Z. One-pot synthesis of biocompatible superparamagnetic iron oxide nanoparticles/hydrogel based on salep: Characterization and drug delivery. Carbohydr Polym 2014;101: 741-751.
29. Batool S, Hussain Z, Niazi MBK, Liaqat U, Afzal M. Biogenic synthesis of silver nanoparticles and evaluation of physical and antimicrobial properties of Ag/PVA/starch nanocomposites hydrogel membranes for wound dressing application. J. Drug. Deliv. Sci. Technol. 2019; 52: 403-414.
30. Palem RR, Kummara MR, Kang T J. Self-healable and dual-functional guar gum-grafted-polyacrylamidoglycolic acid-based hydrogels with nano-silver for wound dressings. Carbohydr. Polym. 2019; 223: 115074.
31. Thakur VK, Thakur MK. Recent trends in hydrogels based on psyllium polysaccharide. J. Clean. Prod. 2014; 89: 1-15.
32. Naushad M, Sharma G, Alothman ZA. Photo degradation of toxic dye using Gum Arabic-crosslinked-poly(acrylamide)/Ni$(OH)_2$/FeOOH nanocomposites hydrogel. J. Clean. Prod. 2019; 241: 118263.
33. Kamaci M. Polyurethane-Based Hydrogels for Controlled Drug Delivery Applications. Eur. Polym. J. 2020;123: 109444.
34. Mandru M, Bercea M, Gradinaru LM, Ciobanu C, Drobota M, Vlad S, Albulescu R Polyurethane/poly (vinyl alcohol) hydrogels: Preparation, characterization and drug delivery. Eur. Polym. J. 2019;118: 137-145.
35. Southall M. Retraction: A polyurethane–chitosan brush as an injectable hydrogel for controlled drug delivery and tissue engineering. Polym. Chem. 2021;12: 2346.
36. Dalton E, Morris Z, Ayres N. Synthesis and characterization of sulfated-lactose polyurethane hydrogels. Polym. Chem. 2022;13: 2933-2940.
37. Ahmad R, Mirza A. Synthesis of Guar gum/bentonite a novel bionanocomposite: Isotherms, kinetics and thermodynamic studies for the removal of Pb (II) and crystal violet dye. J. Mol. Liq. 2018;249: 805-814.
38. Yan L, Li S, Yu H, Shan R, Du B, Liu T. Facile solvothermal synthesis of Fe_3O_4/ bentonite for efficient removal of heavy metals from aqueous solution. Powder. Powder. Technol. 2016;301: 632-640.
39. Karimi MA, Hatefi Mehrjardi A. Nanotechnology Laboratory. (4ed.). Tehran: payamresan, 2011.
40. Viezzer Ch, Mazzuca R, Machado DC, Forte MMC, Ribelles JLG. A new waterborne chitosan-based polyurethane hydrogel as a vehicle to transplant bone marrow mesenchymal cells improved wound healing of ulcers in a diabetic rat model. Carbohydr. Polym. 2020; 231: 115734.
41. Frydrych M, Roman S, Green N.H, Neil S.M, Chen B. Thermoresponsive, stretchable, biodegradable and biocompatible poly(glycerol sebacate)-based polyurethane hydrogels. Polym. Chem. 2015; 6:7974-7987.
42. Mahanta A.K, Senapati S, Maiti P. Polyurethane-Chitosan brush as injectable hydrogel for controlled drug delivery and tissue engineering. Polym. Chem. 2017; 8:6233-6249.
43. Kumari P, Chandran P, Khan SS. Synthesis and characterization of silver sulfide nanoparticles for photocatalytic and antimicrobial applications. J. Photochem. Photobiol. B, Biol. 2014;141:235-240.
44. Sahraei R, Ghaemy M. Synthesis of modified Gum Tragacanth/Graphene Oxide composite hydrogel for heavy metal ions removal and preparation of Silver nanocomposite for Antibacterial Activity. Carbohydr. Polym. 2017; 157: 823-833.
45. Parsamanesh M, Tehrani AD, Mansourpanah Y. Supramolecular hydrogel based on cyclodextrin modified GO as a potent natural organic matter absorbent. Eur. Polym. J. 2017;92:126-136.

Table S1. The effect of the $AgNO_3$ concentration on swelling of hydrogels in different time

t(min)	Swelling $AgNO_3$ 0.0M	Swelling $AgNO_3$ 0.01M	Swelling $AgNO_3$ 0.02M	Swelling $AgNO_3$ 0.03M	Swelling $AgNO_3$ 0.04M	Swelling $AgNO_3$ 0.05M
10	2.54	2.28	1.14	1.24	1.70	0.68
20	2.78	2.88	1.24	1.36	1.78	0.90
30	3.00	3.42	1.36	1.72	1.88	2.62
40	3.16	3.44	1.68	1.84	1.90	2.65
50	3.18	4.10	2.28	1.94	1.96	2.70
60	3.24	4.34	2.32	2.00	2.00	2.76
70	3.36	4.42	2.48	2.04	2.02	2.80
80	3.38	4.50	2.52	2.10	2.08	2.82
90	3.58	4.56	2.82	2.16	2.12	2.94
100	3.70	4.70	2.84	2.60	2.28	2.96
110	3.96	4.72	3.00	2.84	2.42	3.00
120	3.96	4.72	3.00	2.84	2.42	3.00
130	3.96	4.72	3.00	2.84	2.42	3.00

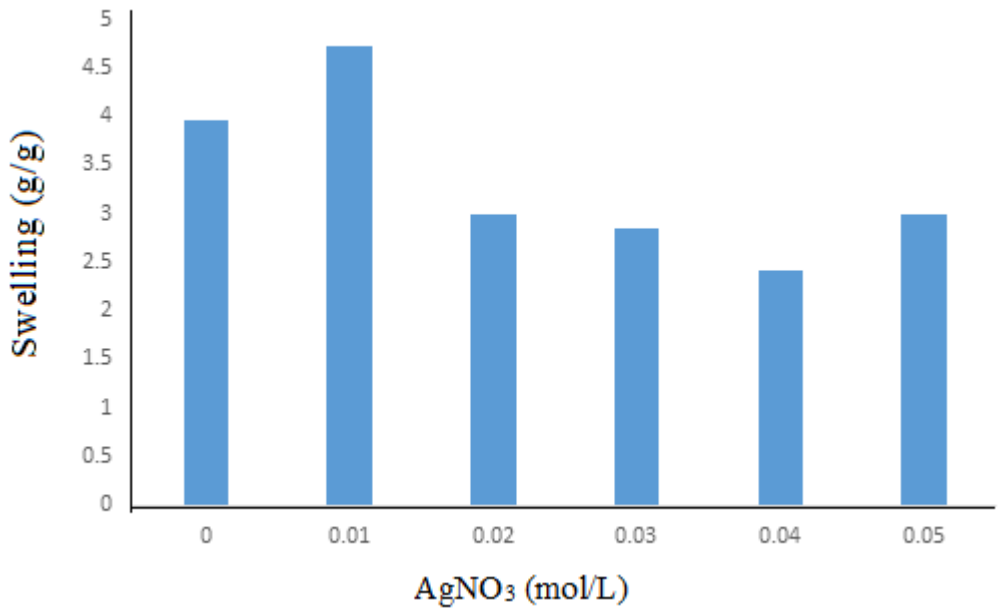

Figure S1. Swelling profile of Balangu/ Fe_3O_4/Ag_2S/polyurethane in different concentration of $AgNO_3$ for 2h

Table S2. Results of Propranolol release from the drug loaded hydrogel at 37 °C.

t(min)	$AgNO_3$ 0 M	$AgNO_3$ 0.01 M	$AgNO_3$ 0.02 M	$AgNO_3$ 0.03 M	$AgNO_3$ 0.04 M	$AgNO_3$ 0.05 M
5	0.15/0.002675[a]	0.17/0.003115	0.19/0.003555	0.16/0.002895	0.18/0.003335	0.13/0.002234
10	0.26/0.005096	0.2/0.003775	0.26/0.005096	0.29/0.005756	0.24/0.004656	0.15/0.002675
15	0.37/0.007517	0.26/0.005096	0.31/0.006196	0.36/0.007297	0.31/0.006196	0.24/0.004656
20	0.49/0.010159	0.35/0.007077	0.40/0.008178	0.44/0.009058	0.34/0.006857	0.31/0.006196
25	0.52/0.010819	0.39/0.007957	0.41/0.008398	0.47/0.009718	0.40/0.008178	0.39/0.007957
30	0.59/0.01236	0.56/0.0117	0.75/0.015882	0.59/0.01236	0.48/0.009939	0.44/0.009058
35	0.71/0.015001	0.69/0.014561	0.78/0.016542	0.71/0.015001	0.55/0.011479	0.52/0.010819
40	0.74/0.015662	0.74/0.015662	0.84/0.017863	0.78/0.016542	0.62/0.01302	0.59/0.01236
45	0.89/0.018964	0.75/0.015882	0.85/0.018083	0.8/0.016983	0.72/0.015222	0.60/0.01258
50	0.91/0.019404	0.81/0.017203	0.90/0.019184	0.81/0.017203	0.73/0.015442	0.65/0.013681
55	0.95/0.020284	0.9/0.019184	0.92/0.019624	0.84/0.017863	0.81/0.017203	0.70/0.014781
60	0.96/0.020505	0.97/0.020725	0.95/0.020284	0.9/0.019184	0.86/0.018303	0.73/0.015442
65	0.96/0.020505	0.97/0.020725	0.95/0.020284	0.9/0.019184	0.88/0.018744	0.76/0.016102
70	0.96/0.020505	0.97/0.020725	0.95/0.020284	0.9/0.019184	0.90/0.019184	0.81/0.017203
75	-	-	-	-	0.98/0.020945	0.84/0.017863
80	-	-	-	-	0.98/0.020945	0.85/0.018083
85	-	-	-	-	0.98/0.020945	0.88/0.018744
90	-	-	-	-	-	0.90/0.019184
95	-	-	-	-	-	0.90/0.019184
100	-	-	-	-	-	0.90/0.019184

[a] UV/ Released of $C_{16}H_{21}NO_2$(g/L)

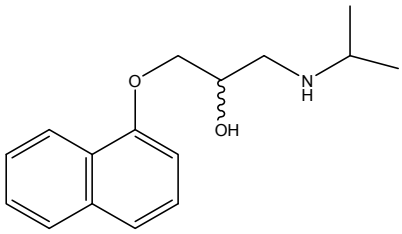

Figure S2. Structure of 1-(1-methylethylamino)-3-(1-naphthyloxy) propan-2-o

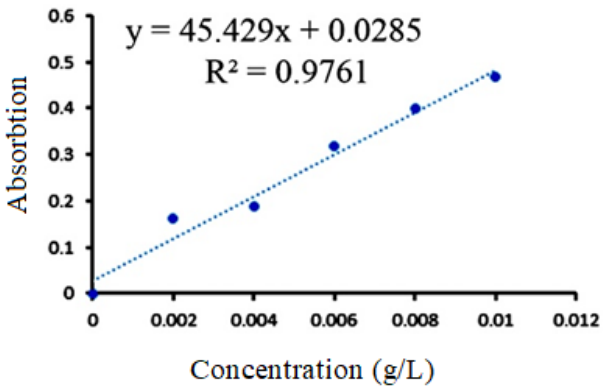

Fig S3. The calibration curve of propranolol

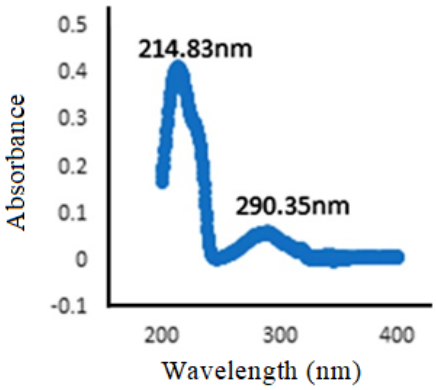

Figure S4. UV–visible spectra of the propranolol